Biomaterials Science

ROYAL SOCIETY OF CHEMISTRY

PAPER

Cite this: *Biomater. Sci.*, 2025, **13**, 1683

Branched silver–iron oxide nanoparticles enabling highly effective targeted and localised drug-free thrombolysis

Karla X. Vazquez-Prada, [a,b,c] Shehzahdi S. Moonshi,[a,c] Yuao Wu, [a,c] Karlheinz Peter,[d,e,f] Xiaowei Wang,[d,e,f] Zhi Ping Xu[b] and Hang Thu Ta *[a,c]

Received 17th August 2024,
Accepted 3rd February 2025

DOI: 10.1039/d4bm01089b

rsc.li/biomaterials-science

Ultrasound has been widely used as an external stimulus to trigger drug release from nanomaterials in thrombosis treatment. Here, we introduce a novel strategy leveraging nanomaterials not for drug delivery, but for enhancing US-induced thrombolysis. This innovative strategy is particularly significant, as thrombolytic drugs inherently pose a risk of systemic bleeding. We combined branched silver–iron oxide nanoparticles (AgIONPs) with low-intensity focused ultrasound to evaluate their thrombolytic potential. Binding assays in in vitro human blood clots and in a thrombosis mouse model confirmed that the targeted AgIONPs specifically bound to thrombi. Upon ultrasound activation, AgIONPs facilitated thrombolysis via two key mechanisms: hyperthermia driven by the nanoparticle-mediated thermal conversion, and mechanical shear forces induced by ultrasound. The combination of AgIONPs and US generated a synergistic thrombolytic effect, demonstrating significant efficacy in both *in vitro* and *in vivo*.

Introduction

Thrombosis and its complications constitute 80% of cardiovascular deaths and continue to be the most common causes of mortality and morbidity in the world.[1–4] Thrombosis refers to the formation of a blood clot within blood vessels that prevents blood from flowing normally in the circulatory system.[5–11] The half-life of antithrombotic agents in the body is usually only a few minutes, and large quantities need to be administrated for an effective treatment. Thus, antithrombotics are associated with several adverse effects including risk of serious to lethal bleeding.[12]

In recent years, there has been a quest for new thrombosis therapies with safer profiles, more targeted and precise strategies, and better treatment outcomes.[13,14] Novel strategies to fight thrombosis focus on identifying new potential targets, developing personalized medicines, combined antithrombotic therapy, and strategies to mechanically remove thrombus.[15] Relatively old technologies such as ultrasound (US), a widely used clinical imaging modality,[16] have been remodeled and reemerged for local treatment of thrombosis. US or high-intensity focused US itself can cause physical changes in acoustic cavitation and microstreaming, forming gas-filled bubbles that will produce shock waves and high-speed fluid micro-jets.[17] Trubestein *et al.* demonstrated in 1976 that acoustic energy could lyse clots *in vitro* and *in vivo* without injuring surrounding tissues.[18] There has been increasing evidence that indicates US thrombolysis might be an effective and safe approach to fight thrombosis while decreasing bleeding complications.[19,20]

US has also been employed as an external stimulus to break drug-encapsulated microbubbles, micelles, and liposomes for drug release. Siyu Wang *et al.* used US to trigger the release of tissue plasminogen activator (tPA) from a nanoparticle-shelled microbubble for thrombolysis.[21] The ultrasound stimulation also improves the drug penetration into thrombi. Some of the advantages of using US to stimulate a nanosystem include its non-invasiveness, preciseness, simple operation and few side effects.[22] Another study showed that the combination of ultrasound and urokinase or streptokinase enhanced lysis rate by an average of 25% compared to lysis with thrombolytic agents alone.[23] These studies indicate the great potential of US for thrombosis treatment.

Here, we report a different strategy. We innovatively employed nanomaterials not for drug delivery but for enhancing US-induced thrombolysis. Nanoparticles were used as seeds for nucleation of microbubbles and reduce the pressure needed to induce cavitation, resulting in more efficient throm-

[a]*School of Environment and Science, Griffith University, Nathan, Queensland 4111, Australia. Tel: +61 (7) 3735 5384; E-mail: h.ta@griffith.edu.au; https://hangta.group/https://experts.griffith.edu.au/27034-hang-ta*
[b]*Australian Institute for Bioengineering and Nanotechnology, the University of Queensland, St Lucia, Queensland 4072, Australia*
[c]*Queensland Micro- and Nanotechnology, Griffith University, Nathan Campus, Brisbane Queensland 4111, Australia*
[d]*Baker Heart and Diabetes Institute, Melbourne, Victoria 3004, Australia*
[e]*Department of Cardiometabolic Health, University of Melbourne, Bio21, Victoria 3052, Australia*
[f]*Department of Medicine, Monash University, Victoria 3004, Australia*

bolysis. In this study, we synthesized and functionalized a branched silver–iron oxide nanoparticle (AgIONP) for ultrasound-activated thrombolysis. This is the first study employing nanomaterials to accelerate cavitation-assisted sonothrombolysis without the use of any drugs. This innovative approach is a significant development as any use of thrombolytic drugs comes with the risk of systemic bleeding side-effect.

Experimental section

Materials

Iron(III) chloride, iron(II) sulfate, silver nitrate, hydroxylamine 50%, sodium hydroxide, COOH-PEGSH (7500 g mol^{-1}), mPEGSH (6000 g mol^{-1}), Tris-HCl, Triton-X 100, and calcium chloride dihydrate were purchased from Sigma-Aldrich. Phosphate-buffered saline (PBS), (1-ethyl-3-(3-dimethylaminopropyl) carbodiimide hydrochloride) (EDC), trisodium citrate (TSC), and micro bichinchoninic (BCA) protein assay were purchased from ThermoFisher Scientific. The single chain antibody (scFv) used for targeting activated platelets (SCE5), control non-targeting scFv (mut) and sortase A enzyme were produced by a collaborator in Baker Heart and Diabetes Institute (Melbourne, Australia). Gly-CONH-PEG3-N3 and dibenzoazacyclooctyne (DBCO) used were from Click Chemistry Tools. Other materials include Cy5 (Lumiprobe), PrestoBlue (Invitrogen), and Actin FSL (Dade Siemens). Water used in all experiments was deionized water. Blood products were obtained from healthy volunteers with informed consents (Australian Red Cross) under the guidelines of human ethics approved by Griffith University human ethics committee (approval number: 2021/598).

Synthesis and characterization of SCE5-AgIONPs

The core of AgIONPs is formed by a cluster of iron oxide nanoparticles (IONPs) synthesized using a co-precipitation method of iron II and III in constant stirring and under constant nitrogen flow at 80 °C. NaOH (1 M) was added dropwise into an aqueous solution of $FeCl_3{\cdot}6H_2O$ (0.2 M) and $(NH_4)_2Fe(SO_4)_2{\cdot}6H_2O$ (0.1 M) until pH reached 12. IONPs were then washed (6000*g*, 15 min) with 1 M HCl and coated with 0.1 M TSC at 80 °C for 6 h under stirring (600 rpm). The citrate-coated IONPs were collected *via* centrifugation at 8000 rpm for 6 min, dialysed against deionized water and stored at 4 °C.

The growth of a silver coating on the IONPs was conducted using a seeding method previously described.[24] Briefly, an aqueous solution of IONPs (0.144 mg of iron) was mixed with hydroxylamine 50% (20 μL) and trisodium citrate (70 μL of 1.14%). Five aliquots of $AgNO_3$ (50 μL each, 6.348 mM) were added to the solution every 10 minutes, followed by the addition of 75 μL of TSC (1.14%). AgIONPs were then collected by centrifugation at 4000*g* for 6 min and redispersed in deionized water.

The resulting nanoparticles were then coated with mPEG-SH and COOH-PEG-SH to increase stability and allow biofunctionalization with targeting ligands. The mass ratio between mPEG-SH and COOH-PEG-SH was 2.5 : 1, and mass ratio between mPEG-SH and Ag was 5 : 1. AgIONPs (35.6 μg of Ag – 45 μL of 1 mg mL^{-1} AgIONPs stock), were first incubated at room temperature with 89 μL of mPEG-SH (2 mg mL^{-1}). After 1 h, 35.6 μL of COOHPEG-SH (2 mg mL^{-1}) was added into the mixture and left for overnight incubation. The PEG@AgIONPs were washed three times with water at 1000 *g* for 6 min until excess polymer was removed. PEG@AgIONPs were conjugated with Cy5 and a targeting scFv (SCE5) for targeting activated platelets in the thrombi. A non-binding mutated non-targeting scFv (mut) was used as a negative control. A more detailed description of the conjugation can be found in the ESI of Vazquez-Prada *et al.*[24]

Characterization of the nanoparticles

The average hydrodynamic size and size distribution were estimated with dynamic light scattering (DLS) (Zetasizer Nano ZS, Malvern). The size and morphology of the nanoparticles was then confirmed by Transmission Electron Microscopy (TEM) images. The proportion and distribution of the metals in AgIONPs were evaluated with Energy Dispersive X-ray Spectroscopy (JEOL-JEM-1010 Transmission Electron Microscope). Inductively coupled plasma-optical emission spectroscopy (ICP-OES) (Optima 8300DV ICP-OES from PerkinElmer) further corroborated the concentrations of silver and iron in the sample. The absorbance spectra of AgIONPs were determined using a CARY 60 UV-vis spectrophotometer (300–900 nm).

Binding assays to *in vitro* thrombi

The nanoparticle's efficacy for binding *in vitro* human thrombi was tested using *in vitro* human clots. For this purpose, $CaCl_2$ (5 μL, 1 M) and actin (12 μL) were added to an Eppendorf tube. After mixing both chemicals, 180 μL of human fresh frozen plasma (FFP) (Australian Red Cross Service) was added and carefully mixed by reverse pipetting. The mixture was incubated for 1 h at 37 °C. The resulting clots were then washed for 30 min at room temperature with PBS 7.4 and subtle rotation (200 rpm). The clots were incubated with the nanoparticles suspended in PBS pH 7.4 (concentration of SCE5-AgIONPs = 0.1 mg mL^{-1}) for 15 min under rotation. After incubation, the clots were washed three times with PBS for a total of 45 min. The clots were fixed with 4% PFA and imaged using a Sapphire machine on fluorescence mode (Cy5 filter).

In vitro optimization of US settings for thrombolysis

Blood from healthy volunteers (Australian Red Cross) was used for developing *in vitro* human thrombi. Blood was centrifuged (15 min at 250*g*) to collect red blood cells (RBC; pellet) and platelet-rich plasma (PRP; supernatant). A solution of 95% PRP and 5% RBC was made in order to mimic the composition of human arterial thrombus.[25] $CaCl_2$ (5 μL, 1 M) was added to 200 μL of this mixture and was left at room temperature for 15 min. The glass vials were weighed before and after the experiment to estimate the thrombolysis percent. The initial and final temperature were also recorded with a thermal camera (FLIR, US). The resulting thrombi were incubated with 100 μL of different concentrations of the nanoparticles and optimization of the settings was made. PBS was used as the

control in all of the experiments. The thrombi were treated with a low-power ultrasound probe (Hainertec, Suzhou Co., Ltd) with different power intensities for 1.5, 2.5, and 3.5 min. The liquid in the glass after treatment was removed and the decrease in the clot's mass was calculated for each thrombus. The percentage decrease in the thrombus mass was normalized against that of the control.

Cytotoxicity, hemocompatibility and biodistribution of AgIONPs

The effect of AgIONPs on the viability of endothelial (SVEC-4-10) cells was determined using PrestoBlue assay, which measures the amount of resorufin that is reduced from resazurin in live cells. SVEC cells were cultured in RPMI media supplemented with 10% fetal bovine serum, 100 U mL^{-1} penicillin, and 100 μg mL^{-1} streptomycin, at 5% CO_2 at 37 °C. The cells were seeded in a 96 well plate (6000 cells per well) for 24 h and then incubated with different concentrations of nanoparticles in PBS for 24 and 48 h. PrestoBlue solution (10 μl) was added to the wells for 30 min and fluorescence intensity was measured in a microplate reader (PerkinElmer; emission 560 nm; excitation 590 nm).

The hemocompatibility assays were performed in triplicates and within 3 hours of collecting blood from healthy volunteers in 3.2% sodium citrate containing tubes. Whole blood (285 μL) was incubated with 15 μL of different concentrations of SCE5-AgIONPs for 4 and 24 h with mild shaking at 37 °C. After incubation, the suspension was centrifuged (1000 rpm for 15 min) and the supernatant was collected. Absorbance using a microplate reader (FLUOstar Omega, BMG LABTECH) was measured at 545 nm. The percentage of hemolysis was estimated using eqn (1):

$$\text{Hemolysis}\,(\%) = \frac{\text{OD sample} - \text{OD negative control}}{\text{OD positive control} - \text{OD negative control}} \times 100 \quad (1)$$

The biodistribution and accumulation of SCE5-AgIONPs were evaluated after the *in vivo* experiments were finalized (single intravenous injection of SCE5-AgIONPs at 8 mg kg^{-1}). All animal studies were in accordance with the Guidelines for Care and Use of Laboratory Animals of the University of Queensland (approval number: AIBN/420/19/CAI and 2020/AE000350). Main organs (heart, liver, spleen, lung, and kidneys) of targeted (SCE5-AgIONPs) and non-targeted (mut-AgIONPs) groups were collected. Fluorescence imaging was obtained using the IVIS Spectrum (ex = 650; em = 670) (PerkinElmer) and fluorescence intensities were analysed using the region of interest (ROI) function and calculated using IVIS Lumina X5 Living Image Software.

In vivo fluorescence imaging and US-enhanced thrombolysis using SCE5-AgIONPs

All animal experiments were conducted at The Centre for Advanced Imaging at The University of Queensland (Protocols were approved by The University of Queensland Ethics Committee; No. AIBN/420/19/CAI and 2020/AE000350). C57/BL6 male mice (26–28 g; Animal Resources Centre, ARC – Western Australia) were anaesthetised with a mixture of ketamine : xylazine (100 : 10 mg per kg body weight) by intraperitoneal injection. Hair shedding cream was used to remove the fur covering cheeks, neck, and chin of the mice. $AlCl_3$-induced thrombosis model was used for all *in vivo* experiments.[24] Briefly, a small incision was made on the neck of the mouse. The left carotid artery was isolated and placed on top of a 1 cm × 2 mm plastic paper. The artery was washed with PBS and carefully dried with a kimwipe. A 1 mm × 2 mm filter paper was soaked in a 9% solution of $AlCl_3$, and placed on top of the artery for 30 seconds after removing the excess of $AlCl_3$. The artery was then washed thoroughly with PBS. The blood flow was measured before and after the induction of thrombi. Mice were randomly divided into three groups: control (PBS), targeted (SCE5-AgIONPs), and non-targeted (mut-AgIONPs) (n = 5, 100 μL, 8 mg of AgIONPs per kg).

In vivo binding efficiency was tested using fluorescence imaging (ex = 650; em = 670) (IVIS Spectrum PerkinElmer). Images were taken at time 0 (pre-injection) and 20 min after the injection. Fluorescence intensity and total radiance efficiency were calculated using the IVIS software.

The therapeutic efficacy was evaluated immediately after the fluorescence imaging using two different approaches. The first one served to calculate the restoration of blood flow *in vivo* and the second one was for measuring the area of thrombus remaining in the arteries after the treatment. For the first method, a flowmeter probe (Transonic) was used at 160 Hz to measure the blood flow in the artery of each mouse before induction of thrombus (F_0), immediately after the induction (F_1), and after the treatment (F_2) with a 0.5 mm flowmeter probe (Transonic). The blood restoration percent was calculated between the groups using the following formula:

$$\text{Blood restoration}\,(\%) = \frac{(F_2 - F_1)(100)}{F_0} \quad (2)$$

The clotted artery was treated with the low-power US probe using the optimized settings from the *in vitro* experiments (2.5 min, 35% or 2 W cm^{-2}, 2 cycles). All experiments were performed after 1 h of thrombus induction. The temperature before and after each cycle was obtained using infrared thermal camera (FLIR C2).

For the thrombolysis evaluation using the second method, the carotid arteries of the mice were retrieved before euthanasia, washed with PBS, and fixed with 4% paraformaldehyde (PFA). The arteries were then processed and cut into cryosections (5 μm) and were further stained with Masson's trichrome. The prepared histological slides were observed under the microscope (Olympus Upright FL Microscope BX63). The remaining area was quantified and analysed with ImageJ.

Statistical analyses

Results are presented as mean ± standard deviation from at least triplicate experiments performed in a parallel manner. The differences among the groups were analysed with one-way or two-way analysis of variance (ANOVA) using GraphPad Prism, at confidence levels of 95% and 99%. The methods used in this study for *post-hoc* analyses were Bonferroni and

Tukey. For *in vivo* experiments, the sample size was at least $n = 5$. All graphs were plotted using GraphPad Prism 9, with $*p < 0.05$ considered significant while $**p < 0.01$, $***p < 0.001$, and $****p < 0.0001$ to be very significant.

Results and discussion

Synthesis, characterization, and binding efficiency of SCE5-AgIONPs

Iron oxide nanoparticles (IONPs) were synthesized and served as the core of our nanosystem. Resulting IONPs showed good stability, were homogeneously dispersed (PDI = 0.178), and had a hydrodynamic size of 32.7 nm and a *z*-potential of −31.4 mV (Fig. 1a and b). Rehman *et al.* demonstrated that growing silver onto IONPs was possible by using a seeding method.[26] The mechanism of the coating relies on electrostatic interactions between the surface of the oxide (*i.e.* iron oxide) and the silver ions. The IONPs themselves, along with TSC and hydroxylamine helped reduce the silver ions seeded on the IONPs surface, as suggested by the literature.[27] The IONPs were successfully coated with silver to form AgIONPs, as shown by the increase in size (127.2 nm), change in *z*-potential (−27.2 mV) and the shift of absorbance to the NIR. Fig. 1d and

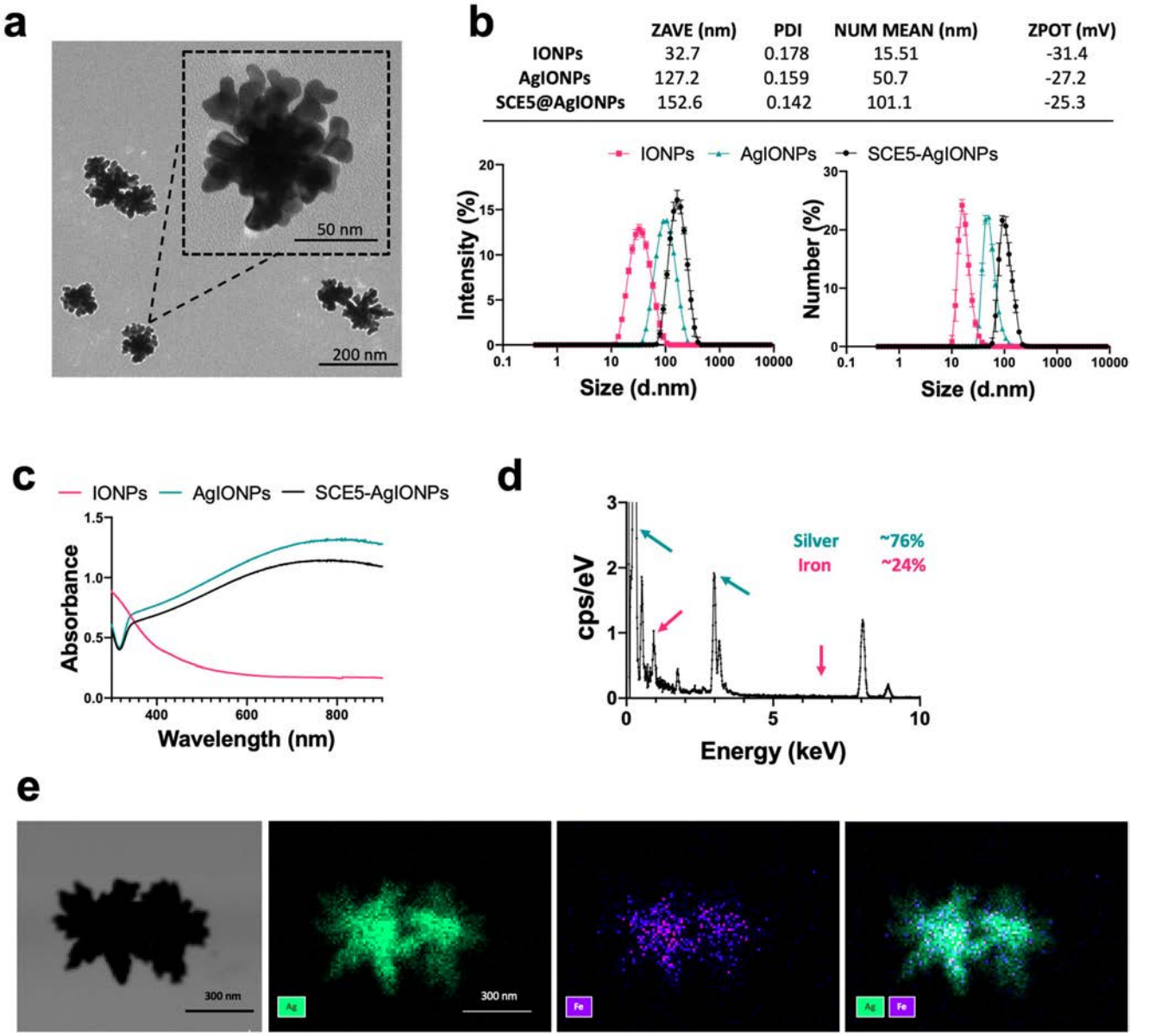

Fig. 1 Characterization of SCE5-AgIONPs. (a) TEM image of the nanoparticles showing an asymmetrical nanorose-like shape. (b) Size distribution (intensity and number by dynamic light scattering), PDI, and zeta potential of the three nanoparticles synthesized in this study. (c) Change in the absorbance spectra of IONPs, AgIONPs, and SCE5-AgIONPs, indicating coating of the nanosystem. (d) EDS spectra of the nanoparticles and (e) elemental mapping, showing presence and distribution of silver (teal in EDS/green in map) and iron (pink in EDS/purple in map).

e show the EDS spectra and elemental mapping from SCE5-AgIONPs, which corroborates the presence of both metals constituting the basis of the nanosytem. A further decrease in *z*-potential and increase in size then suggested successful conjugation of the resulting AgIONPs with a single-chain antibody (SCE5-AgIONPs), as well as a slight decrease in the intensity of the absorbance spectra (Fig. 1b and c).

TEM images of SCE5-AgIONPs suggest the nanoparticles have an asymmetrical nanorose-like shape and confirmed the size and PDI of the nanoparticles (Fig. 1a). Importantly, our results in size, PDI, and zeta potential agree with other IONPs in the literature that have been coated with noble metals such as gold and silver using a similar method.[26,28] The asymmetrical shape has been previously reported to shift the absorbance of nanoparticles to the NIR and to provide optical features to nanosystem such as a strong surface plasmon resonance.[29] The successful branched morphology of the nanoparticle (Fig. 1a) was achieved because the cluster of iron oxide nanoparticles at the core acted as a catalyst for the silver coating, resulting in an asymmetrical shape that enhanced its therapeutic efficiency. Non-spherical nanoparticles have increased surface roughness, which promote the formation of voids that trigger cavitation, ultimately compromising the mechanical integrity of the thrombus and aiding in its dissolution.[30] Asymmetric nanoparticles are known to interact differently with acoustic waves than spherical ones due to their irregular geometry and larger surface area, which facilitates better alignment with the ultrasound field and enhances cavitation effects.[31,32] This shape-dependent behaviour leads to more efficient acoustic cavitation,[33] where the formation and collapse of microbubbles generate localized mechanical forces that disrupt thrombi. The unique structure of the AgIONPs allows for more controlled oscillation under ultrasound, intensifying the cavitation effect and enabling more effective thrombolysis compared to spherical nanoparticles. Additionally, non-spherical nanoparticles offer improved circulation stability and tissue penetration, allowing them to accumulate more effectively at the thrombus site and maximize therapeutic outcomes.[34,35] Furthermore, we envision developing the AgIONPs into a theranostic nanoparticle, where the IONPs would also serve as contrast agents for MRI,[36–41] enabling real-time monitoring of the treatment and enhancing both its therapeutic and diagnostic capabilities. Although MRI property of this NP is not strong enough to image tiny thrombus in this study, our previous study showed efficient MRI of this NP for imaging tumor.[42]

After synthesis, AgIONPs were conjugated to Cy5 and biofunctionalized with an engineered single-chain antibody (SCE5) targeting the activated form of glycoprotein IIb/IIIa, a highly expressed integrin in thrombi.[43] The same antibody but with a mutation in the binding site (mut) was conjugated to the nanoparticles and served as a non-binding control for all experiments. Both antibodies were conjugated to an azide (N_3) peptide, as shown in Fig. 2a. Moreover, we conjugated DBCO to the nanoparticles by activating the –COOH groups of AgIONPs with EDC, which has been previously described to promote click chemistry reaction with N_3 *via* strain-promoted alkyne–azide cycloaddition (Fig. 2a).[44–46]

Targeting efficiency was tested through binding assays with *in vitro* human clots. Fig. 2b shows representative brightfield and fluorescence images of *in vitro* human clots after incubation and three washing cycles. The clots incubated with the targeting nanoparticles (SCE5-AgIONPs) were visibly darker than the controls, suggesting there was accumulation of the dark silver nanoparticles. Importantly, the darker spots visible on the brightfield image correlate with the fluorescence signal when imaging with the Cy5 filter. The mut-AgIONPs incubated clots exhibited a slight change in color whereas the control clots remained white. The small binding of mut-AgIONPs to the clots can be explained by nonspecific binding and interactions between the antibodies to components of the clot such as activated platelets or fibrin.[47] Nonetheless, quantitative analysis of the fluorescence intensity of each group shows that there was no statistical difference between the PBS group and the non-targeted group ($P = 0.131$), whereas the targeted group had significant higher fluorescence than either control group ($P < 0.0001$) (Fig. 2c).

SCE5-AgIONPs can lyse thrombi *in vitro* upon US exposure

We used an *in vitro* model of human thrombi to test the ability of the nanoparticles to enhance thrombolysis and to identify the optimal US settings for *in vivo* assays. Results show that treatment with SCE5-AgIONPs + US was able to lyse thrombi in a dose dependent matter. The percentage in thrombolysis was greater when increasing the intensity of the US, the time of exposure and the number of treatment cycles (Fig. 3a and b). It is important to note that the optimized settings were selected by taking into consideration both parameters shown in Fig. 3a, percentage of thrombolysis and increase in temperature. The settings where the temperature increase was higher than 13 °C (~50 °C) were not considered, as it has been previously reported that a temperature higher than 50 °C can cause burns to human tissue.[48] The desired change in temperature for this study was ~10 °C, since that is the optimal temperature increase for causing thrombolysis without harming surrounding tissues.[49] With this rationale, we selected the optimized settings for SCE5-AgIONPs + US treatment to be a concentration of total nanoparticle mass of 0.2 mg mL^{-1}, an intensity of 35% (2 W cm^{-2}), with an exposure of 2.5 minutes for two cycles.

As shown by Fig. 3, thrombolysis depends on the ultrasound intensity, time of exposure, number of cycles and concentration of the nanoparticle. The optimized settings obtained for *in vivo* studies agree with others in the literature, who have demonstrated how low intensity US (1–4 W cm^{-2}) can enhance thrombolysis.[19] It is important to highlight that previous studies indicate that the mechanism of ultrasound (US) is primarily mechanical. However, there are some reports suggesting that when combined with thrombolytic agents like tPA, US can enhance the transport of enzymes to the thrombus.[18,19]

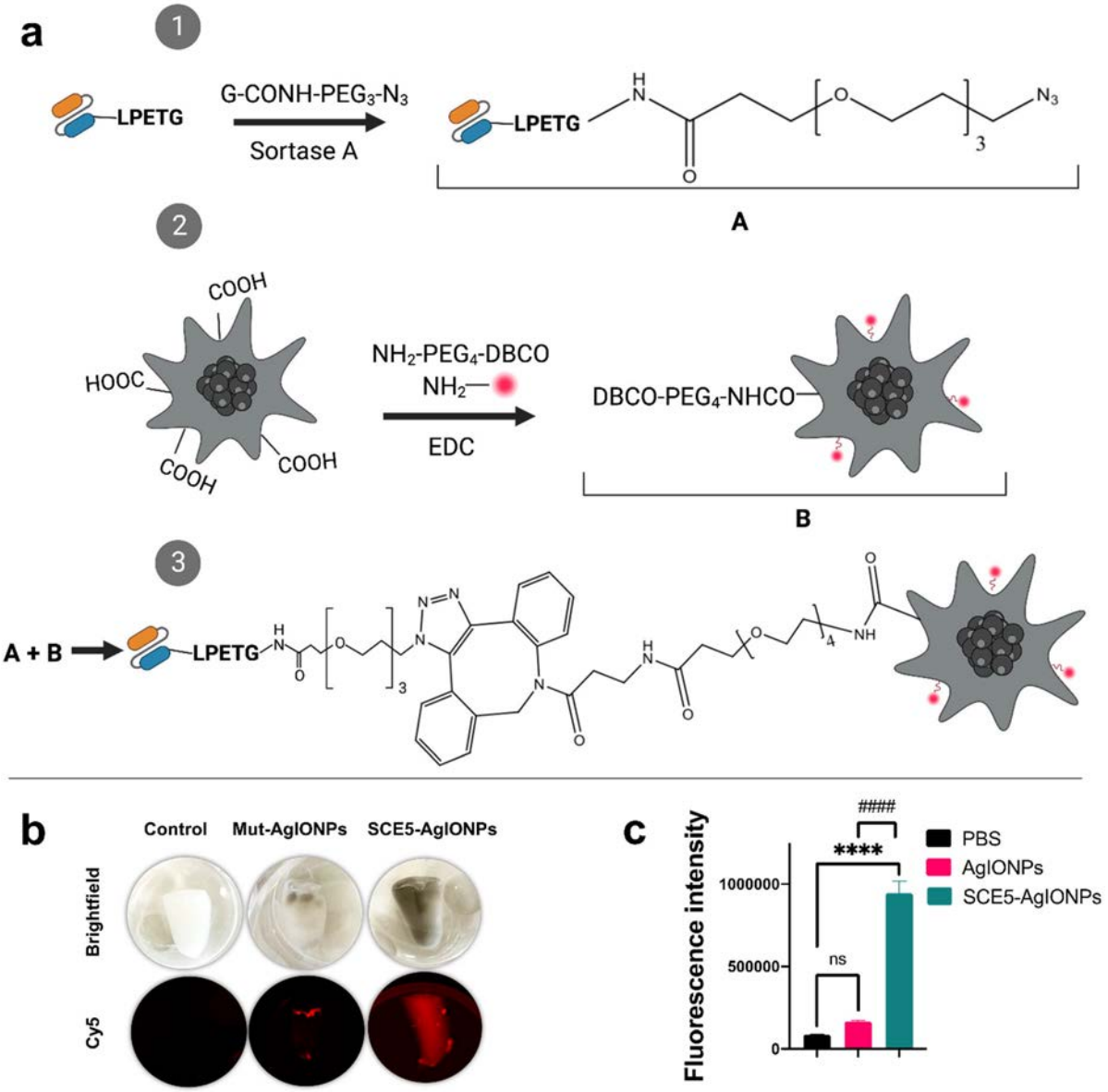

Fig. 2 Binding efficiency of the nanoparticles to *in vitro* human thrombus. (a) Scheme illustrating the steps required for conjugation of Cy5 and scFv. First, an azide group is attached to the antibody *via* Sortase-mediated conjugation (1), and in a separate reaction, the carboxylic groups on the surface of AgIONPs are activated with EDC and conjugated to the amine groups of the Cy5 and the DBCO (2). The DBCO from the nanoparticle reacts with the azide group attached to the antibody *via* click chemistry (3). For non-targeted nanoparticles, the scFv is replaced by the non-targeted antibody (mut), which has the same structure except for the binding region that has been replaced with a non-binding fragment. (b) Representative brightfield and fluorescence images of thrombi incubated with the three groups, a greater number of nanoparticles in targeted group as indicated by the dark layer around the clots and the quantitative analysis (c) of the fluorescence intensities of each group. All statistical analyses were done with one-way ANOVA and Tukey *post-hoc* test ($n = 3$; ns = $p > 0.01$, #### and **** = $p < 0.0001$). Control = PBS; non-targeted = mut-AgIONPs; targeted = SCE5-AgIONPs.

Briefly, US exposure leads to disruption of large fibrin bundles into smaller bundles, causing a reduction in flow resistance and enhancing enzymatic induced thrombolysis by exposing more binding sites for thrombolytic agents.[50] Unlike our study, these published studies do not report a dramatic increase in temperature. In addition, neither the SCE5-AgIONPs nor the US alone promote a significant decrease in the thrombi mass, suggesting the enhancement of thrombolysis might be a mechanism produced by both elements and to be a result of synergy (Fig. 3).

The thrombolytic activity can't be entirely attributed to US, since the thrombolytic effects of the controls with US treatment and no nanoparticles did not show a high percentage of lysis. The groups treated with AgIONs + US had the highest thrombolysis percentage, suggesting the thrombolysis shown here was probably a synergistic effect between the US and the

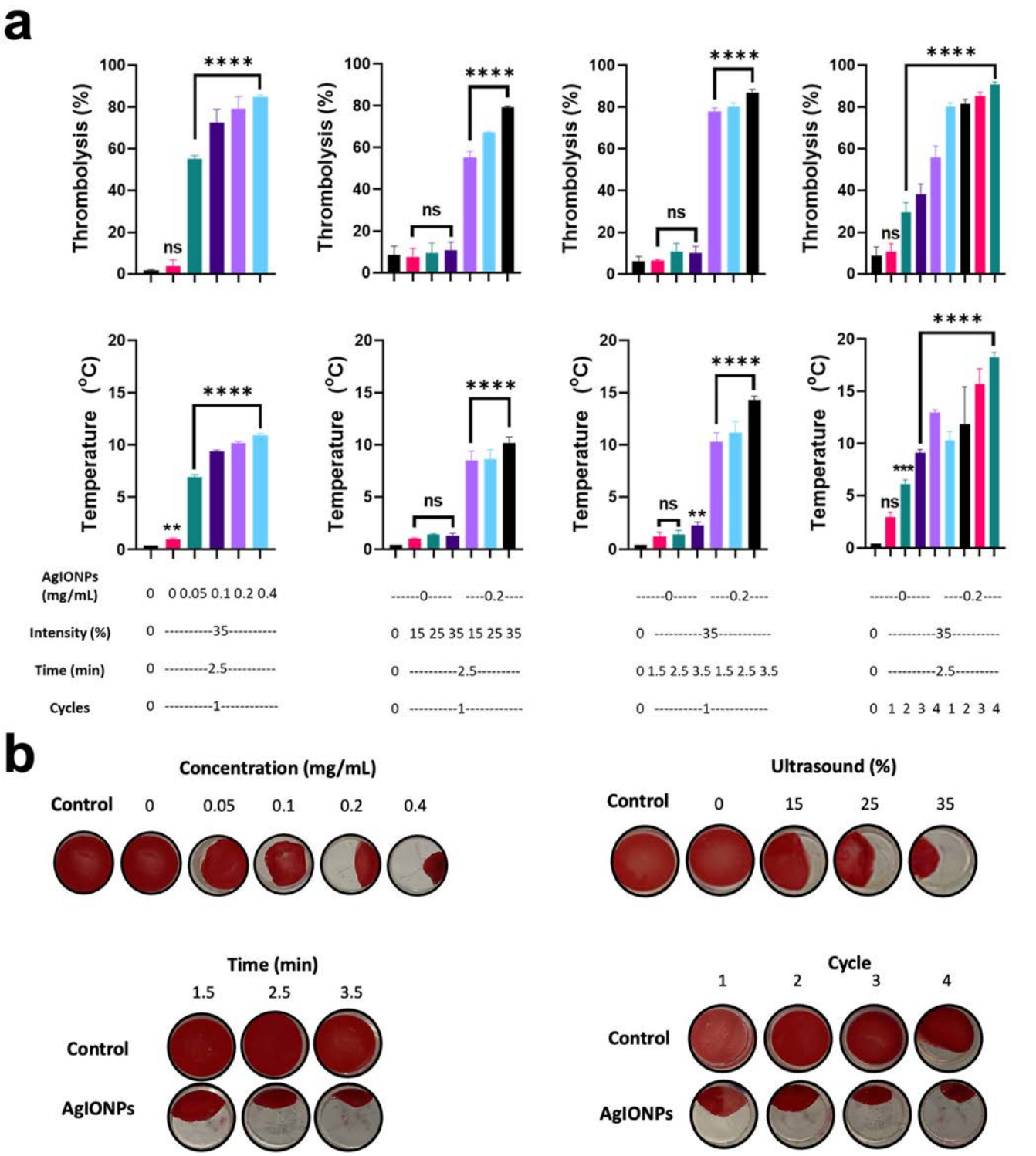

Fig. 3 SCE5-AgIONPs and US treatment can lyse synergistically *in vitro* human blood clots. (a) Optimization of ultrasound settings (SCE5-AgIONPs concentration, intensity of US, time of treatment, number of cycles) for animal experiments. (b) Illustrative images of *in vitro* clots after treatment with each combination of settings (n = 3; ns = $p > 0.05$, ** = $p < 0.01$, *** = $p < 0.001$, and **** = $p < 0.0001$).

nanoparticles. It has been shown that the therapeutic efficiency of US mediated hyperthermia can be improved with sonosensitizers.[51] Most sonosensitizers used for enhancing therapeutic outcomes include exogenous absorbers such as dyes, microbubbles, and more recently nanoparticles.[52] Nanoparticles can prevent potential damage to surrounding tissues while enhancing thermal ablation.[53] The enhancement in deposition of acoustic energy has been found to be achieved

by increasing the attenuation and dissipation of that acquired acoustic energy within the local disease area in the form of heat.[51] We hypothesize that the mechanism of action includes mechanical/acoustic cavitation and enhancement of thermal thrombolysis, both triggered by US and enhanced by SCE5-AgIONPs.[54]

The first mechanism relies on the generation of acoustic streaming and cavitation caused by the US. Cavitation is a thermodynamic process that consists of the growth and collapse of microbubbles and occurs when a homogeneous liquid suffers a drop in pressure below its saturated vapor pressure at a certain temperature.[55] Vapor transport and residual gas pockets in the tissue trigger bubble nucleation, followed by bubble growth and collapse.[56] It has been previously described that these bubble dynamics inflict mechanical injury to blood clots whilst avoiding damage to surrounding tissue.[57] Previous reports show that nanoparticles are able to reduce the pressure needed to induce cavitation and can serve as seeds for nucleation of microbubbles.[58] When a particle is dispersed in a liquid, it provides a nucleation site for the cavitation bubble to form.[59]

The nanoparticles' surface roughness and ability to reduce the cavitation threshold not only facilitate the formation of cavitation nuclei but also increase the number of bubbles when the liquid is exposed to US and reduce the time needed for treatment.[60] Therefore, ablation of thrombi can be achieved by generating cavitating bubbles in the blood vessel using US pulses with acoustic pressures that induce mechanical damage. We speculate that US exposure triggered cavitation and mechanically disrupt the surface of the blood clot by lysing cells and loosening the fibrin network.[23,32,61–64] The second mechanism involves hyperthermia. US hyperthermia is a medical treatment that consists of increasing the temperature of tissues to cause thermal ablation.[65] The millimetric precision of the acoustic beam minimizes the damage of surrounding tissues in comparison to other external stimuli for triggering hyperthermia.[51] Ultrasound mediated hyperthermia consists in the conversion of acoustic/mechanical energy into thermal energy.[52] Heating is mainly due to absorption of ultrasound energy.[66] Briefly, the ultrasound beam is absorbed by the tissue as it propagates through the focal point causing an increase in the local temperature.[67] The asymmetrical silver–iron oxide nanoparticles used for this study have previously shown to have strong photothermal efficiency conversion when activated by an external trigger.[24,42] The thermal conversion of SCE5-AgIONPs in our study is evidenced by the change in temperature (Fig. 3a) after treatment. Notably, the change in temperature is even more evident when the concentration of the nanoparticle is increased, suggesting SCE5-AgIONPs has a crucial role in this effect. Nonetheless, understanding the differences between US-mediated hyperthermia and the photothermal effect is crucial for this study. Both approaches have shown therapeutic efficacy through temperature elevation, but each have their own energy sources, mechanism, penetration depths and specificity in targeting tissues.[68] US-mediated hyperthermia functions by converting acoustic energy into heat through mechanical vibrations and friction, which facilitates deep tissue penetration and targeted heating.[69] This approach is particularly effective in thrombosis for thrombus ablation and improving the delivery of therapeutic agents. In contrast, the photothermal effect relies on light absorption by photosensitive materials, producing localized heating that primarily impacts superficial tissues.[70–72]

Safety studies, biocompatibility, and biodistribution of SCE5-AgIONPs

The toxic effects of the nanoparticles were evaluated *in vitro* and *ex vivo* to ensure compatibility of the nanoparticles for clinical translation. The effects of SCE5-AgIONPs to whole blood were evaluated using a colorimetric assay that measures the amount of hemoglobin in the supernatant of blood incubated with the nanoparticles. Hemolysis percentage increases if the supernatant obtained from low-speed centrifugation of the blood after incubation with the nanoparticles showed a red-like color and absorbance at 545 nm. Fig. 4a shows clear supernatants obtained immediately after centrifugation of blood incubated by 4 h, suggesting no cell lysis. The quantitative analysis (Fig. 4b) show the nanoparticles had minimal toxic effects on the blood with hemolysis percentage below 2%, which is within the threshold of biosafety parameters.[73]

Cytotoxicity of AgIONPs was assessed with CHO cells and endothelial cells by using PrestoBlue assay, a colorimetric assay that quantifies viable cells. Our results show there was no significant decrease in the viability of CHO cells even after 24 and 48 h after incubation with AgIONPs at the concentrations used in this study, as illustrated in Fig. 4c. Cell viability of endothelial cells after SCE5-AgIONPs + US treatment (Fig. 4d) did not show a significant decrease (200 μg of SCE5-AgIONPs per mL, 2 W cm^{-2}, 2.5 min on, 2.5 min off, 2 cycles), suggesting clinical translation potential of the NPs.

To evaluate the compatibility and distribution of SCE5-AgIONPs in the body, *ex vivo* analyses of histological cuts and fluorescence imaging of organs were performed. The collected vital organs included heart, lungs, liver, kidneys, and spleen from treated mice. Microscopy images of histological cuts showed no apparent toxic effects in the morphology or composition of organs from mice treated with the non-targeted and targeted nanoparticles (Fig. 4e). The biodistribution of the nanoparticles was estimated with the total radiant efficiency from the organ images. Fig. 4f shows the accumulation of SCE5-AgIONPs and mut-AgIONPs mainly in the livers and kidneys. The size of the nanoparticles is bigger than that of the nanoparticles that can be cleared *via* the renal mechanism.[74] Although more studies need to be performed to confirm the specific metabolic pathway they go through for clearance from the body, we can hypothesize because of their size and metallic nature that they follow the reticuloendothelial system or the tubular excretion, an alternative to the renal mechanism for larger nanoparticles.[75] Fig. 4g revealed the nanoparticles did not produce any toxic effects on major organs based on analysis of H&E-stained sections.

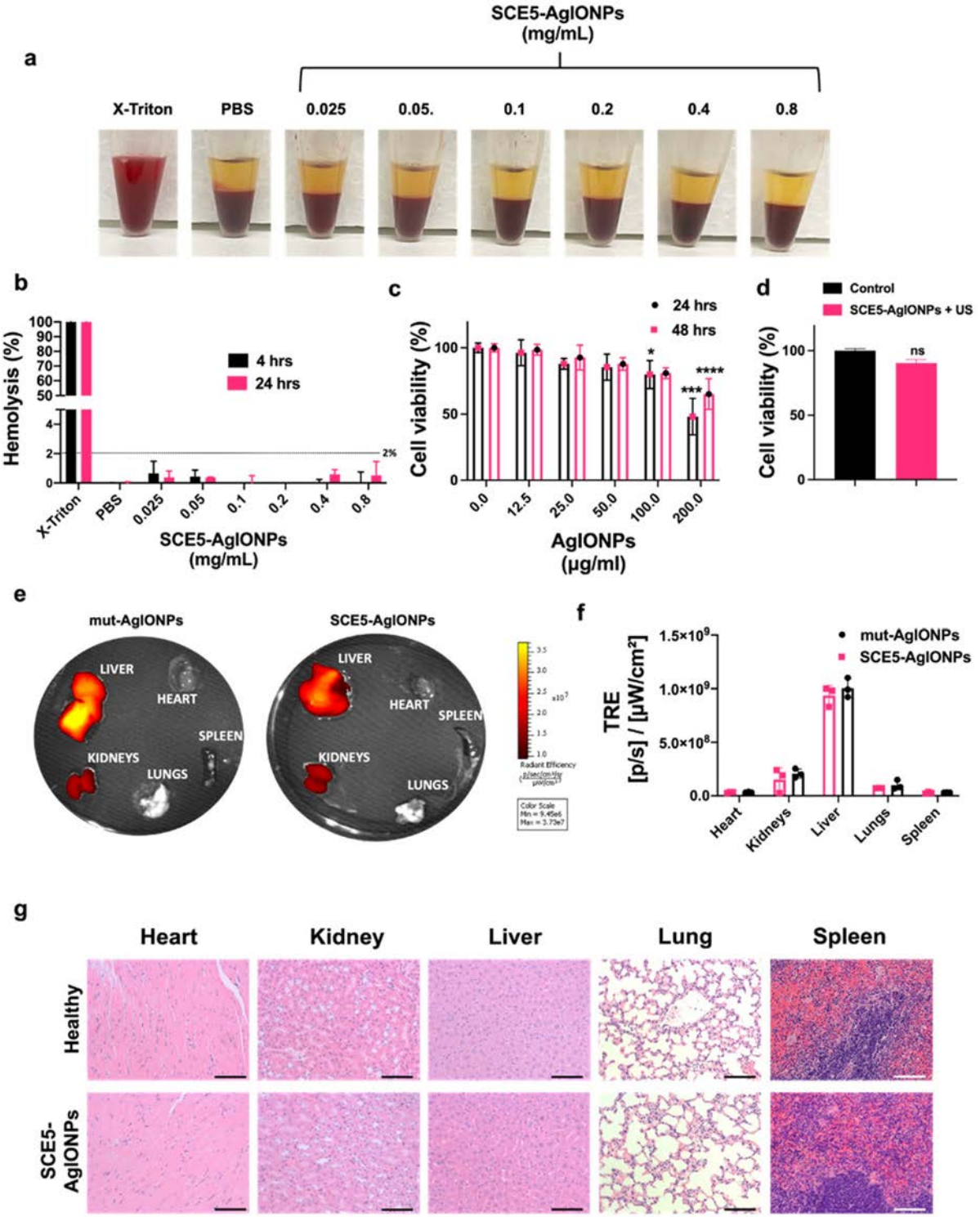

Fig. 4 Biosafety of AgIONPs. (a) Whole blood after 4 h incubation with SCE5-AgIONPs. Supernatant is visibly clear. (b) Quantitative analysis confirms a non-significant hemolysis percentage for 4 and 24 h, suggesting no adverse effects in red blood cells from the nanoparticles (n = 3). (c) Cytotoxicity of CHO after incubation for 24 and 48 h with nanoparticles showing no drastic decrease in cell viability at the dose used in this work. (d) Cell viability of endothelial cells after SCE5AgIONPs + US treatment did not show a significant decrease (200 μg of SCE5-AgIONPs per mL, 2 W cm^{-2}, 2.5 min on, 2.5 min off, 2 cycles). (e) *Ex vivo* fluorescence images of important organs and (f) analysis of their total radiance efficiency, showing no statistical differences between both groups and accumulation of both nanoparticles mostly in the liver. (g) Histology of important organs collected from the control mice and the mice treated with SCE5-AgIONPs, both showing no apparent toxicity after the treatment (scale bar = 100 μm; n = 3; * = $p < 0.05$, *** = $p < 0.001$, and **** = $p < 0.0001$).

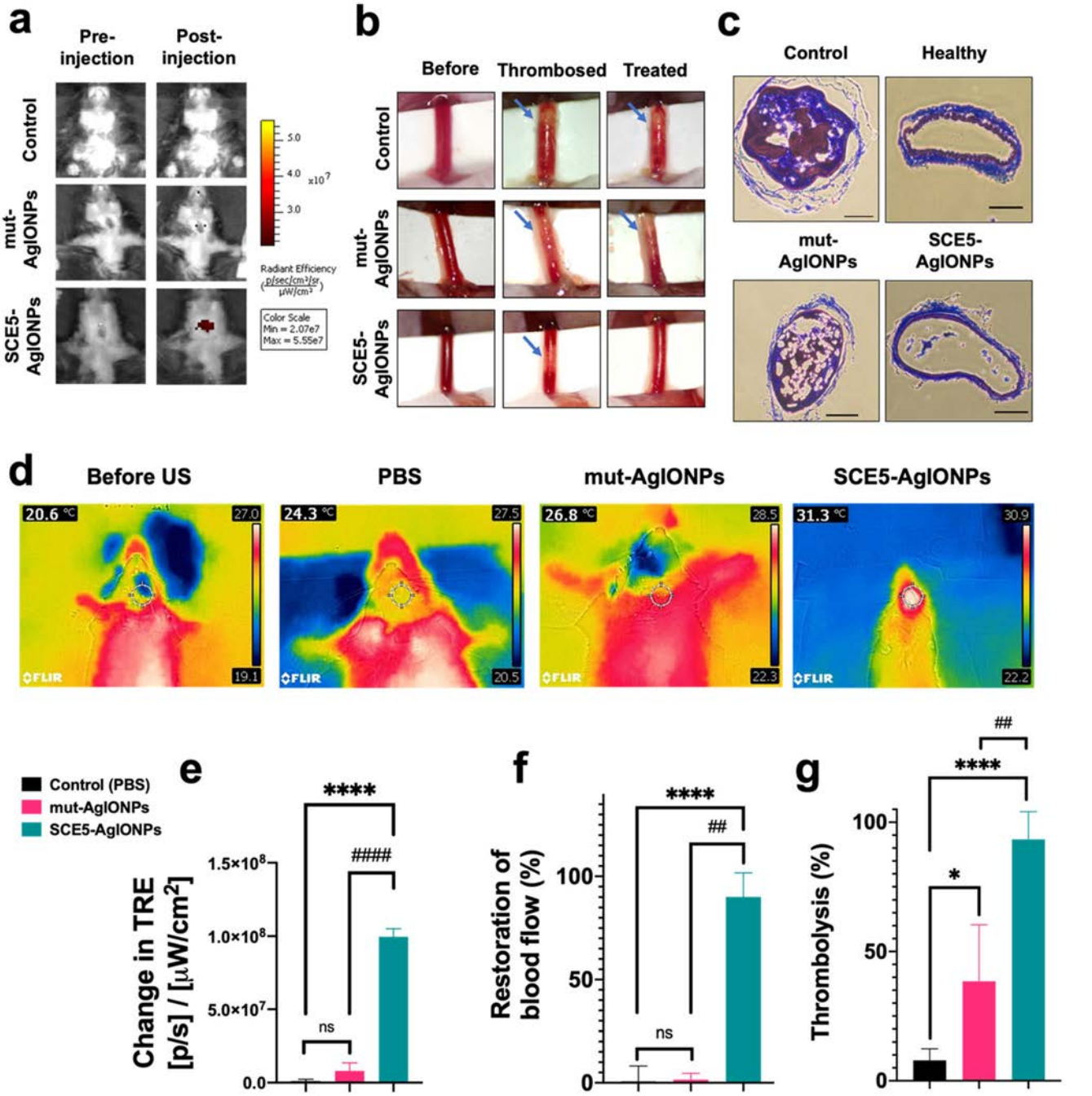

Fig. 5 SCE5-AgIONPs effectively targets thrombi and enhances US thrombolysis in vivo. The nanoparticles (SCE5-AgIONPs and mut-AgIONPs) were injected (8 mg whole NP per kg of body weight) (n = 4). (a) Fluorescence images before and 20 min after iv injection of the nanoparticles. Total radiance efficiency of the mice treated with the targeted nanoparticle show a visible increase in fluorescence (neck area) suggesting only significant accumulation of targeted nanoparticles in the arterial thrombi. (b) Images of the arteries before thrombi induction, after thrombi induction and after treatment with US. Visible clots in the images are pointed with an arrow. All the arteries were successfully thrombosed but only the targeted group showed a visible decrease in the clot size after treatment. (c) Representative microscope images of histological cuts of arteries post-treatment, showing less thrombi area (red; Masson's trichrome stain) remaining in targeted group when compared to the controls (scale bar = 100 μm). (d) Thermal images showing temperature after the last treatment cycle. The biggest change in temperature was seen in the targeted group (~10.5 °C) whereas the non-targeted had a change in temperature of ~6 °C. (e, f and g) Graphs and statistical analyses from A, B, and C, respectively, suggesting the targeted group showed a statistical significance in the binding, restoration of blood flow, and thrombolysis percent than the control groups (n = 4, ns = $p > 0.05$, * = $p < 0.05$, ** and ## = $p < 0.01$, *** = $p < 0.001$, **** and #### = $p < 0.0001$).

SCE5-AgIONPs effectively target thrombi and enhances US-thrombolysis *in vivo*

We used an $AlCl_3$ induced thrombosis mouse model for *in vivo* experiments.[24,29,46] Prior to the thrombolysis experiments, we used fluorescence imaging to evaluate accumulation of the nanoparticles to the thrombosed arteries of the mice. Fig. 5a show the fluorescence images before and after iv injection of the nanoparticles. The quantitative measurements of total radiance efficiency of the targeted-treated group after 20 min show an increase in fluorescence whereas no significant increase was shown in the control non-targeted groups ($p < 0.0001$), suggesting that the targeted nanoparticles were able to bind specifically to the thrombi *in vivo* (Fig. 5e).

The protocol used for animal studies was optimized in the *in vitro* thrombolysis experiments using the same US probe with the optimized settings, which were determined to be 2 cycles of 2.5 min with an US intensity of 35% (2 W cm^{-2}). The data gathered from the *in vivo* thrombolysis assay is summarized in Fig. 5. A visual change between microscope images before and after US treatment was observed for targeted nanoparticle group (Fig. 5b). The thermal images after the final cycle indicate the change in temperature for the group treated with SCE5-AgIONPs + US to be ~10.5 °C, ~6 °C for the mut-AgIONPs + US, and ~4 °C for the group with PBS + US (Fig. 5d). The changes in temperature in the groups treated with mut-AgIONPs + US and PBS + US are within the range of what has been described previously to cause mild thrombolysis with US treatment (~5 °C).[76] Nonetheless, for complete restoration of blood flow, the ideal change in temperature for lysing the thrombi without harming any surrounding tissue is ~10 °C.[24,29] Importantly, in this study the artery was inside the body and the outside neck area was exposed to the probe US, without requiring catheter-like devices nor invasive procedures. There was no evidence of damage to the vessel nor the surrounding tissue after US treatment even at the highest change in temperature.

To evaluate the restoration of blood flow, we measured blood flow before thrombosis induction as well as before and after treatment with US using 0.5 mm flow probe, as detailed in the methods section. A restoration of the blood flow of more than 90% was observed in the targeted group whereas no evidence of restoration was seen for both control groups (Fig. 5f). Fig. 5c shows the microscope images acquired from the histology of retrieved arteries. The arteries were stained with Masson's Trichrome, which stains the thrombi in red and the collagen of the vessel in blue. The results from the histology analysis showed that the thrombus area (red) was significantly smaller for the groups treated with SCE5-AgIONPs when compared to mut-AgIONPs ($p < 0.01$) and PBS ($p < 0.0001$) groups. Results from histology show a thrombolysis percentage of ~98% for the targeted group, ~45% for the non-targeted, and <15% for the control group (Fig. 5g). Our *in vivo* findings suggest that the small thrombolysis obtained from the PBS + US group may be caused purely by the mechanical effects of US. Moreover, the thrombolysis in the mut-AgIONPs + US group could be attributed to the effects of US and to the mild hyperthermia due to unspecific binding of mut-AgIONPs.

Conclusion

We identified a new application for our previously described nanoparticle system, which is based on iron and silver demonstrating clot-targeting and efficient treatment of thrombosis. We show that the nanosystem presented can bind specifically to thrombi *in vitro*, and *in vivo* in a thrombosis mouse model. We present evidence that SCE5-AgIONPs can be triggered with ultrasound to generate hyperthermia and induce thrombolysis *in vivo* and *in vitro*. Our results suggest that the treatment of thrombi-targeted SCE5-AgIONPs + US shows excellent thrombolysis *in vitro* and *in vivo* and an almost complete restoration of blood flow *in vivo.* Hemocompatibility assays on whole blood, viability assays on CHO cells, and histology analysis of important organs did not reveal apparent toxic effects, neither of the nanoparticles nor the US itself, thus representing a promising and safe alternative treatment for thrombosis. Future follow-up studies should focus on exploring the possibility of using this nanoparticle as a theranostic agent and monitor the US-triggered therapeutic outcome and increase in temperature in real time. Moreover, studies on hyperthermia combination therapy using simultaneous stimuli such as laser + US might provide evidence of a novel and efficient synergistic treatment for thrombosis. Studying the pharmacology and clearance mechanism of SCE5-AgIONPs to explore its potential translation to the clinic is also paramount for future applications.

Ethics approval

All animal studies were in accordance with the Guidelines for Care and Use of Laboratory Animals of the University of Queensland (approval number: AIBN/420/19/CAI and 2020/AE000350).

Author contributions

KXVP: conceptualization, visualization, methodology, analysis, investigation, writing – original draft. SSM and YW: methodology, writing – review and editing. YW, KP, XW and ZPX: supervision, writing – review and editing. HTT: conceptualization, visualization, methodology, supervision, project administration, funding acquisition, resources, writing – review and editing.

Data availability

The data that support the findings of this study are available from the authors upon reasonable request.

Conflicts of interest

The authors declare no competing financial interest.

Acknowledgements

This work is funded by National Health and Medical Research Council (HTT: APP1146694, APP1182347, APP2002827). KXVP is supported by a PhD scholarship from the University of Queensland. HTT is supported by a Heart Foundation Future Leader Fellowship (102761). KP is supported by a NHMRC Investigator Fellowship. XW is supported by a National Heart Foundation Future Leader Fellowship and a Baker Fellowship. The authors would like to acknowledge the Australian National Fabrication Facility (Queensland Node) access to key items of equipment. The authors acknowledge the facilities and scientific and technical assistance of the National Imaging Facility, a National Collaborative Research Infrastructure Strategy (NCRIS) capability, at the Centre for Advanced Imaging, University of Queensland.

References

1 J. Pircher, B. Engelmann, S. Massberg and C. Schulz, Platelet–neutrophil crosstalk in atherothrombosis, *Thromb. Haemostasis*, 2019, **119**(8), 1274–1282.
2 K. X. Vazquez-Prada, J. Lam, D. Kamato, Z. P. Xu, P. J. Little and H. T. Ta, Targeted molecular imaging of cardiovascular diseases by iron oxide nanoparticles, *Arterioscler., Thromb., Vasc. Biol.*, 2021, **41**(2), 601–613.
3 A. Zia, Y. Wu, T. Nguyen, X. Wang, K. Peter and H. T. Ta, The choice of targets and ligands for site-specific delivery of nanomedicine to atherosclerosis, *Cardiovasc. Res.*, 2020, **116**(13), 2055–2068.
4 J. R. Pickett, Y. Wu, L. F. Zacchi and H. T. Ta, Targeting endothelial vascular cell adhesion molecule-1 in atherosclerosis: drug discovery and development of vascular cell adhesion molecule-1–directed novel therapeutics, *Cardiovasc. Res.*, 2023, **119**(13), 2278–2293.
5 B. Engelmann and S. Massberg, Thrombosis as an intravascular effector of innate immunity, *Nat. Rev. Immunol.*, 2013, **13**(1), 34–45.
6 F. Akther, J. Zhang, H. D. N. Tran, H. Fallahi, H. Adelnia, H. P. Phan, *et al.*, Atherothrombosis-on-Chip: A Site-Specific Microfluidic Model for Thrombus Formation and Drug Discovery, *Adv. Biol.*, 2022, **6**(7), e2101316.
7 F. Akther, D. Sajin, S. S. Moonshi, J. Pickett, Y. Wu, J. Zhang, *et al.*, An intimal-lumen model in a microfluidic device: potential platform for atherosclerosis-related studies, *Lab Chip*, 2025, **25**, 354–369.
8 F. Akther, D. Sajin, S. S. Moonshi, Y. Wu, K. X. Vazquez-Prada and H. T. Ta, Modeling Foam Cell Formation in A Hydrogel-Based 3D-Intimal Model: A Study of The Role of Multi-Diseases During Early Atherosclerosis, *Adv. Biol.*, 2024, **8**(4), e2300463.
9 F. Akther, H. Fallahi, J. Zhang, N. T. Nguyen and H. T. Ta, Evaluating thrombosis risk and patient-specific treatment strategy using an atherothrombosis-on-chip model, *Lab Chip*, 2024, **24**(11), 2927–2943.
10 H. T. Ta, N. P. Truong, A. K. Whittaker, T. P. Davis and K. Peter, The effects of particle size, shape, density and flow characteristics on particle margination to vascular walls in cardiovascular diseases, *Expert Opin. Drug Delivery*, 2018, **15**(1), 33–45.
11 F. Akther, H. D. Tran, J. Zhang, N.-T. Nguyen and H. T. Ta, Lab-on-a-chip (lab-on-a-phone) for analysis of blood and diagnosis of blood diseases, in *Nanotechnology for Hematology, Blood Transfusion, and Artificial Blood*, Elsevier, 2022, pp. 237–264.
12 C. C. La, S. A. Smith, S. Vappala, R. Adili, C. E. Luke, S. Abbina, *et al.*, Smart thrombosis inhibitors without bleeding side effects via charge tunable ligand design, *Nat. Commun.*, 2023, **14**(1), 2177.
13 Y. Wu, K. X. Vazquez-Prada, Y. Liu, A. K. Whittaker, R. Zhang and H. T. Ta, Recent advances in the development of theranostic nanoparticles for cardiovascular diseases, *Nanotheranostics*, 2021, **5**(4), 499.
14 J. D. McFadyen, M. Schaff and K. Peter, Current and future antiplatelet therapies: emphasis on preserving haemostasis, *Nat. Rev. Cardiol.*, 2018, **15**(3), 181–191.
15 D. R. Phillips, P. B. Conley, U. Sinha and P. Andre, Therapeutic approaches in arterial thrombosis, *J. Thromb. Haemostasis*, 2005, **3**(8), 1577–1589.
16 X. Wang, Y. Gkanatsas, J. Palasubramaniam, J. D. Hohmann, Y. C. Chen, B. Lim, *et al.*, Thrombus-Targeted Theranostic Microbubbles: A New Technology towards Concurrent Rapid Ultrasound Diagnosis and Bleeding-free Fibrinolytic Treatment of Thrombosis, *Theranostics*, 2016, **6**(5), 726–738.
17 A. L. Klibanov, Ultrasound contrast: gas microbubbles in the vasculature, *Invest. Radiol.*, 2021, **56**(1), 50–61.
18 R. J. Siegel and H. Luo, Ultrasound thrombolysis, *Ultrasonics*, 2008, **48**(4), 312–320.
19 C. W. Francis, Ultrasound-Enhanced Thrombolysis, *Echocardiography*, 2001, **18**(3), 239–246.
20 U. Rosenschein, V. Furman, E. Kerner, I. Fabian, J. Bernheim and Y. Eshel, Ultrasound Imaging–Guided Noninvasive Ultrasound Thrombolysis, *Circulation*, 2000, **102**(2), 238–245.
21 S. Wang, X. Guo, W. Xiu, Y. Liu, L. Ren, H. Xiao, *et al.*, Accelerating thrombolysis using a precision and clot-penetrating drug delivery strategy by nanoparticle-shelled microbubbles, *Sci. Adv.*, 2020, **6**(31), eaaz8204.
22 H. Tian, L. Lin, Z. Ba, F. Xue, Y. Li and W. Zeng, Nanotechnology combining photoacoustic kinetics and chemical kinetics for thrombosis diagnosis and treatment, *Chin. Chem. Lett.*, 2021, **32**(12), 3665–3674.
23 H. Luo, W. Steffen, B. Cercek, S. Arunasalam, G. Maurer and R. J. Siegel, Enhancement of thrombolysis by external ultrasound, *Am. Heart J.*, 1993, **125**(6), 1564–1569.

24 K. X. Vazquez–Prada, S. S. Moonshi, Y. Wu, F. Akther, B. W. Tse, K. A. Sokolowski, *et al.*, A Spiky Silver–Iron Oxide Nanoparticle for Highly Efficient Targeted Photothermal Therapy and Multimodal Imaging of Thrombosis, *Small*, 2023, 2205744.

25 J. Viereck, F. L. Ruberg, Y. Qiao, A. S. Perez, K. Detwiller, M. Johnstone, *et al.*, MRI of atherothrombosis associated with plaque rupture, *Arterioscler., Thromb., Vasc. Biol.*, 2005, **25**(1), 240–245.

26 A. Rehman, Y. Wu, H. D. N. Tran, K. Vazquez-Prada, Y. Liu, H. Adelnia, *et al.*, Silver/Iron Oxide Nano-Popcorns for Imaging and Therapy, *ACS Appl. Nano Mater.*, 2021, **4**(10), 10136–10147.

27 S. Wang, F. Liu, Y. Liu, H. Zhou and B. Yan, One Pot Synthesis of Large Gold Nanoparticles with Triple Functional Ferrocene Ligands, *Int. J. Mol. Sci.*, 2021, **22**(5), 2328.

28 L. L. Ma, M. D. Feldman, J. M. Tam, A. S. Paranjape, K. K. Cheruku, T. A. Larson, *et al.*, Small multifunctional nanoclusters (nanoroses) for targeted cellular imaging and therapy, *ACS Nano*, 2009, **3**(9), 2686–2696.

29 N. A. Fithri, Y. Wu, G. Cowin, F. Akhter, H. D. Tran, B. Tse, *et al.*, Gold-iron oxide nanoparticle: A unique multimodal theranostic approach for thrombosis, *Appl. Mater. Today*, 2023, **31**, 101750.

30 M. Gooniband Shooshtari, M. B. Shiran and S. Shirvalilou, The enhancement of therapeutic effects of low-intensity ultrasound with spiky and spherical gold nanoparticles on CT26 cell line; an in vitro study, *Immunopathol. Persa*, 2024, **10**(2), e40596.

31 S. T. Fateh, L. Moradi, E. Kohan, M. R. Hamblin and A. Shiralizadeh Dezfuli, Comprehensive review on ultrasound-responsive theranostic nanomaterials: mechanisms, structures and medical applications, *Beilstein J. Nanotechnol.*, 2021, **12**, 808–862.

32 W. Choi, J. Key, I. Youn, H. Lee and S. Han, Cavitation-assisted sonothrombolysis by asymmetrical nanostars for accelerated thrombolysis, *J. Controlled Release*, 2022, **350**, 870–885.

33 S.-J. Wang, D. Su, Y.-F. Zhu, C.-H. Lu and T. Zhang, The state-of-the-art review on rational design for cavitation assisted photocatalysis, *Mater. Des.*, 2023, **234**, 112377.

34 C. Ma, J. Zhang, T. Zhang, H. Sun, J. Wu, J. Shi, *et al.*, Comparing the Rod-Like and Spherical BODIPY Nanoparticles in Cellular Imaging, *Front. Chem.*, 2019, **7**, 765.

35 K. Entzian and A. Aigner, Drug Delivery by Ultrasound-Responsive Nanocarriers for Cancer Treatment, *Pharmaceutics*, 2021, **13**(8), 1135.

36 J. L. Y. Tang, S. S. Moonshi, Y. Wu, G. Cowin, K. X. Vazquez-Prada, H. D. N. Tran, *et al.*, A methotrexate labelled dual metal oxide nanocomposite for long-lasting anti-cancer theranostics, *Mater. Today Bio*, 2025, **30**, 101377.

37 H. T. Ta, N. Arndt, Y. Wu, H. J. Lim, S. Landeen, R. Zhang, *et al.*, Activatable magnetic resonance nanosensor as a potential imaging agent for detecting and discriminating thrombosis, *Nanoscale*, 2018, **10**(31), 15103–15115.

38 Y. Wu, R. Zhang, H. D. Tran, N. D. Kurniawan, S. S. Moonshi, A. K. Whittaker, *et al.*, Chitosan nanococktails containing both ceria and superparamagnetic iron oxide nanoparticles for reactive oxygen species-related theranostics, *ACS Appl. Nano Mater.*, 2021, **4**(4), 3604–3618.

39 Y. Liu, Y. Wu, R. Zhang, J. Lam, J. C. Ng, Z. P. Xu, *et al.*, Investigating the use of layered double hydroxide nanoparticles as carriers of metal oxides for theranostics of ROS-related diseases, *ACS Appl. Bio Mater.*, 2019, **2**(12), 5930–5940.

40 Y. Wu, G. Cowin, S. S. Moonshi, H. D. Tran, N. A. Fithri, A. K. Whittaker, *et al.*, Engineering chitosan nano-cocktail containing iron oxide and ceria: a two-in-one approach for treatment of inflammatory diseases and tracking of material delivery, *Mater. Sci. Eng., C*, 2021, **131**, 112477.

41 S. S. Moonshi, Y. Wu and H. T. Ta, Visualizing stem cells in vivo using magnetic resonance imaging, *Wiley Interdiscip. Rev.: Nanomed. Nanobiotechnol.*, 2022, **14**(2), e1760.

42 S. S. Moonshi, K. X. Vazquez-Prada, J. Tang, N. J. Westra van Holthe, G. Cowin, Y. Wu, *et al.*, Spiky Silver–Iron Oxide Nanohybrid for Effective Dual-Imaging and Synergistic Thermo-Chemotherapy, *ACS Appl. Mater. Interfaces*, 2023, **5**(36), 42153–42169.

43 X. Wang, J. Palasubramaniam, Y. Gkanatsas, J. D. Hohmann, E. Westein, R. Kanojia, *et al.*, Towards effective and safe thrombolysis and thromboprophylaxis: preclinical testing of a novel antibody-targeted recombinant plasminogen activator directed against activated platelets, *Circ. Res.*, 2014, **114**(7), 1083–1093.

44 S. Wang, G. Li, Z. Liu, Z. Yang, J. He and X.-H. Dong, Facile construction of giant polymeric chains through strain-promoted azide-alkyne cycloaddition, *Polym. J.*, 2023, 1–11.

45 H. T. Ta, S. Prabhu, E. Leitner, F. Jia, D. von Elverfeldt, K. E. Jackson, *et al.*, Enzymatic single-chain antibody tagging: a universal approach to targeted molecular imaging and cell homing in cardiovascular disease, *Circ. Res.*, 2011, **109**(4), 365–373.

46 H. T. Ta, Z. Li, C. E. Hagemeyer, G. Cowin, S. Zhang, J. Palasubramaniam, *et al.*, Molecular imaging of activated platelets via antibody-targeted ultra-small iron oxide nanoparticles displaying unique dual MRI contrast, *Biomaterials*, 2017, **134**, 31–42.

47 M. Sun, M. H. Hao Pontius, S. Yang, T. Pendekanti, S. Raghunathan, J. A. Shavit, *et al.*, Direct delivery of plasmin using clot-anchoring thrombin-responsive nanoparticles for targeted fibrinolytic therapy, *J. Thromb. Haemostasis*, 2023, **21**(4), 983–994.

48 B. E. Pichoff, M. Schydlower and S. R. Stephenson, Children at risk for accidental burns from hot tap water, *Tex. Med.*, 1994, **90**(11), 54–58.

49 K. X. Vazquez-Prada, S. S. Moonshi, Z. P. Xu and H. T. Ta, Photothermal nanomaterials for theranostics of athero-

sclerosis and thrombosis, *Appl. Mater. Today*, 2023, **35**, 101967.
50 M. M. McNally and M. C. Stoner, Blood Clots, Thrombolytics, and the Emerging Role of the EndoWave Catheter, *US Cardiol.*, 2008, **5**(1), 46–48.
51 K. Kaczmarek, T. Hornowski, M. Kubovčíková, M. Timko, M. Koralewski and A. Józefczak, Heating Induced by Therapeutic Ultrasound in the Presence of Magnetic Nanoparticles, *ACS Appl. Mater. Interfaces*, 2018, **10**(14), 11554–11564.
52 E. A. Kwizera, S. Stewart, M. M. Mahmud and X. He, Magnetic Nanoparticle-Mediated Heating for Biomedical Applications, *J. Heat Transfer*, 2022, **144**(3), 030801.
53 L. Trahms, *Colloidal magnetic fluids, Basics, Development and application of ferrofluids*, 2009.
54 M. Varna, M. Juenet, R. Bayles, M. Mazighi, C. Chauvierre and D. Letourneur, Nanomedicine as a strategy to fight thrombotic diseases, *Future Sci. OA*, 2015, **1**(4), FSO46.
55 C. Kim, W. J. Choi, Y. Ng and W. Kang, Mechanically Induced Cavitation in Biological Systems, *Life*, 2021, **11**(6), 546.
56 M. O. de Andrade, R. Haqshenas, K. J. Pahk and N. Saffari, Mechanisms of nuclei growth in ultrasound bubble nucleation, *Ultrason. Sonochem.*, 2022, **88**, 106091.
57 V. A. Khokhlova, J. B. Fowlkes, W. W. Roberts, G. R. Schade, Z. Xu, T. D. Khokhlova, *et al.*, Histotripsy methods in mechanical disintegration of tissue: Towards clinical applications, *Int. J. Hyperthermia*, 2015, **31**(2), 145–162.
58 A. Yildirim, D. Shi, S. Roy, N. T. Blum, R. Chattaraj, J. N. Cha, *et al.*, Nanoparticle-Mediated Acoustic Cavitation Enables High Intensity Focused Ultrasound Ablation Without Tissue Heating, *ACS Appl. Mater. Interfaces*, 2018, **10**(43), 36786–36795.
59 A. Shanei and M. M. Shanei, Effect of gold nanoparticle size on acoustic cavitation using chemical dosimetry method, *Ultrason. Sonochem.*, 2017, **34**, 45–50.
60 A. Sazgarnia, A. Shanei, A. R. Taheri, N. T. Meibodi, H. Eshghi, N. Attaran, *et al.*, Therapeutic effects of acoustic cavitation in the presence of gold nanoparticles on a colon tumor model, *J. Ultrasound Med.*, 2013, **32**(3), 475–483.
61 Q. Wang, D. Jin, B. Wang, N. Xia, H. Ko, B. Y. M. Ip, *et al.*, Reconfigurable magnetic microswarm for accelerating tPA-mediated thrombolysis under ultrasound imaging, *IEEE/ASME Trans. Mechatron.*, 2021, **27**(4), 2267–2277.
62 Z. Wang, Y. Pan, H. Huang, Y. Zhang, Y. Li, C. Zou, *et al.*, Enhanced thrombolysis by endovascular low-frequency ultrasound with bifunctional microbubbles in venous thrombosis: in vitro and in vivo study, *Front. Bioeng. Biotechnol.*, 2022, **10**, 965769.
63 *Ultrasound and Magnetic Dual-Mode Stacked Transducer for Sonothrombolysis with a Combination of Nanodroplets and Magnetic Nanoparticles*, ed. B. Zhang, H. Wu, X. Jiang. 2022 IEEE 22nod International Conference on Nanotechnology (NANO); 4-8 July 2022, 2022.
64 A. S. Hong, J.-S. Chae, S. B. Dubin, S. Lee, M. C. Fishbein and R. J. Siegel, Ultrasonic clot disruption: an in vitro study, *Am. Heart J.*, 1990, **120**(2), 418–422.
65 T. J. Dubinsky, C. Cuevas, M. K. Dighe, O. Kolokythas and J. H. Hwang, High-intensity focused ultrasound: current potential and oncologic applications, *Am. J. Roentgenol.*, 2008, **190**(1), 191–199.
66 G. Sellani, D. Fernandes, A. Nahari, M. F. de Oliveira, C. Valois, W. C. Pereira, *et al.*, Assessing heating distribution by therapeutic ultrasound on bone phantoms and in vitro human samples using infrared thermography, *J. Ther. Ultrasound*, 2016, **4**, 13.
67 G. ter Haar, *Acoust. Surg. Phys. Today*, 2001, **54**(12), 29–34.
68 P. Kaur, M. L. Aliru, A. S. Chadha, A. Asea and S. Krishnan, Hyperthermia using nanoparticles–Promises and pitfalls, *Int. J. Hyperthermia*, 2016, **32**(1), 76–88.
69 P. Tharkar, R. Varanasi, W. S. F. Wong, C. T. Jin and W. Chrzanowski, Nano-Enhanced Drug Delivery and Therapeutic Ultrasound for Cancer Treatment and Beyond, *Front. Bioeng. Biotechnol.*, 2019, **7**, 324.
70 S. S. Moonshi, K. X. Vazquez-Prada, H. Adelnia, N. J. Westra van Holthe, Y. Wu, J. Tang, *et al.*, Polysuccinimide-based nanoparticle: A nanocarrier with drug release delay and zero burst release properties for effective theranostics of cancer, *Appl. Mater. Today*, 2024, **37**, 102150.
71 A. Fromain, J. E. Perez, A. Van de Walle, Y. Lalatonne and C. Wilhelm, Photothermia at the nanoscale induces ferroptosis via nanoparticle degradation, *Nat. Commun.*, 2023, **14**(1), 4637.
72 X. Zhao, K. Guo, K. Zhang, S. Duan, M. Chen, N. Zhao, *et al.*, Orchestrated yolk–shell nanohybrids regulate macrophage polarization and dendritic cell maturation for oncotherapy with augmented antitumor immunity, *Adv. Mater.*, 2022, **34**(9), 2108263.
73 A. Mesdaghinia, Z. Pourpak, K. Naddafi, R. N. Nodehi, Z. Alizadeh, S. Rezaei, *et al.*, An in vitro method to evaluate hemolysis of human red blood cells (RBCs) treated by airborne particulate matter (PM10), *MethodsX*, 2019, **6**, 156–161.
74 H. S. Choi, W. Liu, P. Misra, E. Tanaka, J. P. Zimmer, B. Itty Ipe, *et al.*, Renal clearance of quantum dots, *Nat. Biotechnol.*, 2007, **25**(10), 1165–1170.
75 V. Naumenko, A. Nikitin, K. Kapitanova, P. Melnikov, S. Vodopyanov, A. Garanina, *et al.*, Intravital microscopy reveals a novel mechanism of nanoparticles excretion in kidney, *J. Controlled Release*, 2019, **307**, 368–378.
76 D. Disharoon, D. W. M. Marr and K. B. Neeves, Engineered microparticles and nanoparticles for fibrinolysis, *J. Thromb. Haemostasis*, 2019, **17**(12), 2004–2015.

